RSC Advances

PAPER

View Article Online
View Journal | View Issue

Cite this: *RSC Adv.*, 2025, **15**, 35368

Novel crosslinked recombinant human collagen scaffolds with excellent cytocompatibility and wound healing effect

Yue He,[a] Xin Wang,[b] Yuhong Niu,[a] Jiuna Wang,[b] Xuyuan Yang[a] and Yongai Zhang *[a]

Objective: This study aimed to investigate the physicochemical properties, cytocompatibility, and tissue repair effects of novel crosslinked recombinant human collagen (rCOL) scaffolds. *Methods*: Novel rCOL scaffolds were prepared using EDC/NHS crosslinking and lyophilization. The physicochemical properties of the scaffolds, including the porosity, pore size, crosslinking degree, tensile strength, endotoxin levels, and genotoxicity, were determined. Their cytocompatibility was investigated *in vitro*, and their tissue repair effects were evaluated in a full-thickness skin wound rat model. *Results*: The crosslinked rCOL scaffolds exhibited a three-dimensional structure with a porosity exceeding 90% and a pore size ranging from 50 to 400 μm. The crosslinking degree of scaffolds prepared from 4% and 8% rCOL exceeded 20%, and all scaffolds withstood a tensile load of 2.5 N. Endotoxin levels were <0.5 EU per mL, below the regulatory limit for implantable medical products. No genotoxicity was detected. *In vitro*, the scaffolds exhibited remarkable cell adhesion and proliferation capabilities, with the 4% rCOL scaffold showing the highest capacity. In a full-thickness skin wound rat model, the scaffolds showed superior efficacy in promoting wound healing compared to animal-derived collagen. *Conclusions*: The biocompatibility and tissue repair of crosslinked rCOL scaffolds have excellent biological performance, providing a new material for wound healing applications.

Received 19th June 2025
Accepted 18th September 2025

DOI: 10.1039/d5ra04354a

rsc.li/rsc-advances

1. Introduction

Tissue engineering is a booming field focused on developing innovative solutions for restoring damaged tissues. A biological scaffold is a 3-dimensional (3D) structure made of biomaterials that support cell growth and tissue development. Biological materials derived from natural sources are highly biocompatible, exhibit low immunogenicity, and degrade without releasing toxic compounds, making them ideal for scaffold construction.[1]

Collagen, the main structure protein in the extracellular matrix of connective tissues, plays a key role in wound healing by providing structural support and promoting tissue regeneration. It is widely used as a raw material for constructing biological scaffolds in tissue engineering.[2] The collagen-based scaffolds have suitable spatial structures and porosity, facilitating the proliferation and migration of various types of cells, such as fibroblasts, neurons, vascular endothelial cells, and osteoblasts.[3] In addition, they stimulate angiogenesis at the injury site and surrounding tissues, enhancing blood circulation and accelerating tissue regeneration.[4,5] In an Achilles tendon injury rat model, treatment with a type I collagen sponge completely restored the tendon's biomechanical properties such as tear resistance, without inducing inflammation.[6] However, collagen derived from an animal source may trigger immunogenic reactions and carry a potential risk of disease transmission.

Recombinant human collagen (rCOL), produced through genetic engineering, closely replicates the amino acid sequence of native human collagen. It can be produced at high purity on an industrial scale. Compared to animal source collagen, rCOL is a preferred material for biological scaffold construction due to its reduced immunogenicity and improved water solubility. The primary rCOL subtypes used in medical applications include types I, II, III, V and XVII.[7–9] In this study, type I and III rCOL with patented sequences were used for the design of a chimeric rCOL for the construction of crosslinked biological scaffolds. This chimeric rCOL was enriched with hydrophilic amino acids and engineered to include additional cell adhesion sites incorporating GPP sequences, thereby enhancing its ability to promote cell adhesion and proliferation. Additionally, the distribution and proportion of lysine and glutamic acid were optimized to facilitate amide bond formation during crosslinking, thereby improving the mechanical properties of the scaffold material [SI 1-Patent No: AU202010052422.9].

[a]*School of Nursing and Rehabilitation, Xi'an Medical University, Xi'an, 710021, China. E-mail: zhangyongai@xiyi.edu.cn*

[b]*Medical Research and Development Center, Shaanxi Huikang Bio-Tech Co., Ltd, Xi'an, 710054, China*

Subsequently, the morphology, microstructure, porosity, mechanical strength, genotoxicity, and cell adhesion of these crosslinked rCOL scaffolds were evaluated, along with their endotoxin levels and ability to enhance wound healing. The findings provide valuable data supporting the clinical assessment and application of these novel rCOL scaffolds.

2. Materials and methods

2.1 Preparation of crosslinked rCOL scaffolds

The amino acid sequence of types I and III chimeric rCOL was designed using the human collagen Gly-X-Y repeat sequence as the fundamental repeating unit. The nucleotide sequences of type I and III human collagen were enzymatically cleaved, linked, and subclones into the Pichia Pastoris expression vector. The expression vector was then introduced into the Pichia Pastoris host bacterium using the electrotransformation method. The strain with the highest vector expression was selected using G418 antibiotic screening. After fermentation, high-purity and water-soluble chimeric rCOL (with a purity of over 98% and a protein yield of approximately 15 g per liter of fermentation broth) was isolated from the fermentation supernatant through ultrafiltration, ion exchange chromatography, and freeze-drying. The freeze-drying process followed these parameters: −50 °C for 6 hours, −30 °C for 3 hours, −25 °C for 0.5 hours, −15 °C for 5 hours, −10 °C for 3 hours, 0 °C for 3 hours, 10 °C for 3 hours, and 25 °C for 5 hours, all conducted under a vacuum of 5–15 pa. The resulting rCOL, which appeared as porous scaffolds, was subsequently crosslinked in 0.05 mol per L EDC and 0.01 mol per L NHS for 18 hours, at a reaction temperature of 25 °C. After the reaction was completed, the scaffolds were thoroughly washed and then subjected to freeze-drying, yielding cross-linked scaffold materials.[10]

2.2 Porosity assessment

The crosslinked rCOL scaffolds were weighed (M) and placed in a 25 mL calibrated pycnometer (M_1) containing anhydrous ethanol. After soaking for 10 min, excess ethanol was removed from the calibration line, and the pycnometer was weighed again (M_2). After that, the scaffolds were removed from the pycnometer, and the pycnometer containing the residual ethanol was weighed (M_3). The scaffold porosity was calculated using the following formula: porosity (%) = $(M_2 - M_3 - M)/(M_1 - M_3) \times 100\%$.

2.3 Evaluation of surface morphology and pore size

The surface morphology of the crosslinked rCOL scaffolds was evaluated using Scanning Electron Microscopy (SEM) (200×) (TESCANVEGA 3 SBH, Czech Republic). The sample preparation procedure involved cross-sectioning and gold coating. The pore size was determined from five points per field of view using the Image Pro-Plus analysis software.

2.4 Mechanical strength

The tensile strength of the crosslinked rCOL scaffolds was measured on a Universal Testing Machine (Wuxing Instruments, China). The material was customized to specific dimensions (2 mm × 10 mm × 20 mm), with one end fixed while the other subjected to a tensile force of 2.5 N or 5 N. The force was applied for 1 min, during which measurements were recorded.

2.5 Measurement of crosslinking degree[11]

The crosslinked rCOL scaffolds were weighed and placed in 1 mL of 4% sodium bicarbonate and 1 mL of 0.5% 2, 4, 6-trinitrobenzenesulfonic acid (TNBS). The mixtures were heated in a water bath at 40 °C for 4 h. After that, 3 mL of 6 mol per L hydrochloric acid was added, and the mixtures were heated at 120 °C for 1 h. The resulting solutions were diluted with 5 mL of distilled water and extracted three times with ether, using 20 mL for each extraction. The ether layers were discarded after each extraction, and the aqueous phase (5 mL) was heated in a water bath at 90 °C for 15 min, allowed to cool to room temperature, and diluted with 15 mL of water. After shaking to ensure thorough mixing, the absorbance at 346 nm was recorded. The absorbance at 346 nm was also recorded for uncrosslinked rCOL, which served as a negative control for crosslinking.

The degree of crosslinking was calculated using the following equation: degree of crosslinking (%) = 1 − (absorbance value of crosslinked rCOL scaffold/mass of crosslinked rCOL scaffold)/(absorbance value of uncrosslinked rCOL/mass of uncrosslinked rCOL).

2.6 Ames test

The bacterial reverse-mutation test (Ames test) was performed on a crosslinked scaffold prepared from 8% rCOL, leached with a 0.9% sodium chloride solution and DMSO, using the plate incorporation method,[12] to evaluate its potential mutagenic effects on *Salmonella typhimurium*. In brief, *Salmonella typhimurium* strains TA97a, TA98, TA100, TA102, TA1535 (Molecular Toxicology Inc., USA) were cultured overnight in TSB medium at 37 °C. The following day, the cultures were shaken at 37 °C until a bacterial suspension of about 10^9 cfu mL^{-1} was obtained. Agar plates were heated at 45 °C until the top Agar layer melted. The bacterial suspensions were then added to the melted Agar medium according to the conditions outlined in Table 1. The bacteria suspensions were mixed with the melted Agar, and the mixtures were transferred to a new plate and allowed to solidify. After the top Agar medium solidified, the plate was inverted and cultured at 37 °C for 72 h. After the culture was completed, the growth of background moss was observed, and the number of revertant colonies in each plate was counted.

Under both activated and non-activated conditions (+S9 or −S9), a result was considered positive if the number of revertant colonies in a test sample was at least twice that of the negative control, with a statistically significant dose-dependent response, or if the number of revertant colonies in a test sample was at least twice the negative control at one or more test levels, with reproducibility and statistical significance. Otherwise, the result was considered negative.

Table 1 Ames test conditions[a]

Group	Components	Test sample (mL)	Spontaneous revertant (mL)	Negative control (mL)	Positive control (mL)
−S9	Test solution	0.1	—	—	—
	0.9% sodium chloride/DMSO	—	—	0.1	—
	Positive mutagen	—	—	—	0.1
	10^9 cfu mL; bacteria solution	0.1	0.1	0.1	0.1
	Phosphate buffer	0.5	0.5	0.5	0.5
+S9	Test solution	0.1	—	—	—
	0.9% sodium chloride/DMSO	—	—	0.1	—
	Positive mutagen	—	—	—	0.1
	10^9 cfu mL; bacteria solution	0.1	0.1	0.1	0.1
	Phosphate buffer	0.5	0.5	0.5	0.5

[a] S9, 10% rat liver S9 fraction for the metabolic activation of chemicals; −, no; +, yes; test solution, solution for scaffold extraction (extraction ratio: 3 cm^2: 1 mL, extraction conditions: 50 °C for 72 h); negative control, test solution alone; positive control, 9-aminoacridine, 2-nitrofluorene, sodium azide, mitomycin C, benzo (a) pyrene, and 2-aminoanthracene.

2.7 Bacterial endotoxin detection

The endotoxin levels of the crosslinked rCOL scaffolds were determined using the gel-clot method for bacterial endotoxin testing, as outlined in the Chinese Pharmacopoeia.[13] The experiment procedure included the following steps: (1) test solution preparation: approximately 0.2 g of a crosslinked rCOL scaffold was soaked in 40 mL of bacterial endotoxin test solution (Zhanjiang Bokang, China) at 37 °C for 72 h. (2) Positive control preparation: endotoxin working standard (Zhanjiang Bokang) was added to 1 mL of endotoxin test solution, mixed for 15 min, and diluted to 0.12 EU per mL (the concentration of 2λ) (λ (the lower limit of detection) = 0.06 EU per mL). A blank bacterial endotoxin test solution served as a negative control. (3) Endotoxin level determination: limulus amebocyte lysate (Zhanjiang Bokang) was added to 0.1 mL of scaffold test solution, positive control, negative control, and distilled water, with each condition tested in duplicate. The mixtures were incubated in a water bath at 37 °C for 1 h, after which gel formation was observed. The test was considered valid if both negative controls yielded negative results. If both were positive, the test was deemed invalid. In cases where one negative control was positive and the other negative, a retest was performed.

2.8 Cell adhesion and proliferation

To assess the cell adhesion capacity of the crosslinked rCOL scaffolds, 2×10^5 L929 cells in the logarithmic growth stage were inoculated onto a scaffold with a dimension of 20 mm^2. After 1 h incubation at 37 °C, 1 mL fresh medium was added, and the mixture was incubated for another 22 h at 37 °C. The scaffold was gently rinsed with PBS three times, transferred into 1 mL of fresh medium containing 10% (volume fraction) MTT reagent (10 mg mL^{-1}), incubated at 37 °C for 4 h, and centrifuged. The supernatant was discarded, and the scaffold was incubated in 150 μL DMSO on a micro oscillator for 10 min. The optical density (OD) at 490 nm was recorded. To assess cell proliferation, L929 cells were cultured with the crosslinked rCOL scaffold as above. Cell proliferation within the scaffold was determined using the MTT method 1, 2, 3, 5, and 7 days after cell inoculation.

2.9 Rat model of skin wound repair

Animals were provided by animal experiment center of Medical College of Xi'an Jiaotong University (animal certificate number: SCXK2018-001). Studies involving animals were approved by the Science and Technology Ethics Committee of Xi'an Medical University (approval No. XYLS2025158). SD rats (male, 200 ± 20 g, $n = 6$) were anesthetized with intraperitoneal 3% sodium pentobarbital (45 mg kg^{-1}). The animals' backs were shaved using electric clippers. A skin sampler (15 mm in diameter) was used to create three full-thickness skin excisions, each with a diameter of 15 mm and an approximate area of 1.8 cm^2. The three wounds were treated with the implantation of a crosslinked rCOL scaffold (A), animal-derived collagen (commercially available product) (B), and untreated control group (C), respectively. The treatment materials were cut to match the size of the wound, applied to the wound area, and secured with an adhesive outer dressing. The wounds were photographed immediately after the procedure, as well as on days 7 and 14 post-operation. Specimens were collected and fixed with 4% paraformaldehyde on day 14. Hematoxylin eosin (HE) and Ki-67 staining were performed on paraffin sections as described below.

2.10 HE staining

The fixed tissue samples were embedded in paraffin and cut into 5–8 μm sections. The paraffin sections were sequentially processed through xylene dewaxing and gradient ethanol dehydration, and final washing with distilled water. The sections were stained with hematoxylin for 5 min, differentiated in 1% hydrochloric acid ethanol for 3–5 s, and rinsed with tap water for 30 min. After that, the sections were stained with 0.5% eosin for 2–4 min and washed with distilled water. After dehydration in gradient ethanol, the sections were immersed in xylene to achieve transparency. Neutral gum was used to seal the sections.

2.11 Ki-67 staining

The fixed tissue sections were dehydrated in gradient ethanol and treated with xylene to achieve transparency. Following thermal antigen retrieval, the sections were incubated with anti-

Ki-67 antibody (1 : 1000, Cat No: 28074-1-AP, Proteintech) at room temperature for 30 min. After washing, the sections were further incubated with a secondary antibody (1 : 2000; HRP-goat anti-rabbit IgG (H + L), Thermo Fisher, Cat. No. 31460), followed by development with DAB staining solution (Proteintech, Cat. No. pr30018). The sections were immersed in hematoxylin staining solution and incubated at room temperature for 1–2 minutes to stain the cell nuclei blue. After differentiation with 1% hydrochloric acid in ethanol, the sections were washed with PBS buffer and placed in xylene for 10 minutes. A suitable amount of mounting medium was added, and a coverslip was placed over the sections. The expression of Ki-67 was detected under a microscope (brown indicates positive). Five regions were selected from each section for imaging, and the positive areas were analyzed using image J image analysis software.

2.12 Statistical analysis

The results are presented as mean ± standard deviation (Mean ± SD). All data were analyzed using SPSS software (v19.0). Comparisons between groups were performed using the *t*-test. A *P* value of less than 0.05 was deemed statistically significant.

3. Results and discussion

3.1 Appearance and microstructure of the crosslinked rCOL scaffolds

The crosslinked rCOL scaffolds prepared under different crosslinking conditions had different appearance, material density, and mechanical strength (Fig. 1A–C). Scaffold A exhibited a white appearance with easily noticeable surface pores, and its overall structure was relatively loose and soft to the touch. Scaffold B had a bright white appearance with a uniform structure and felt more compact compared to scaffold A. Scaffold C exhibited the highest material density and superior mechanical strength. SEM analysis revealed a 3D interconnected porous structure in all scaffolds. Scaffold A′ (crosslinked rCOL at 2% concentration) exhibited relatively large pores, scaffold B′ (crosslinked rCOL at 4% concentration) displayed a uniform distribution of medium-sized pores, and

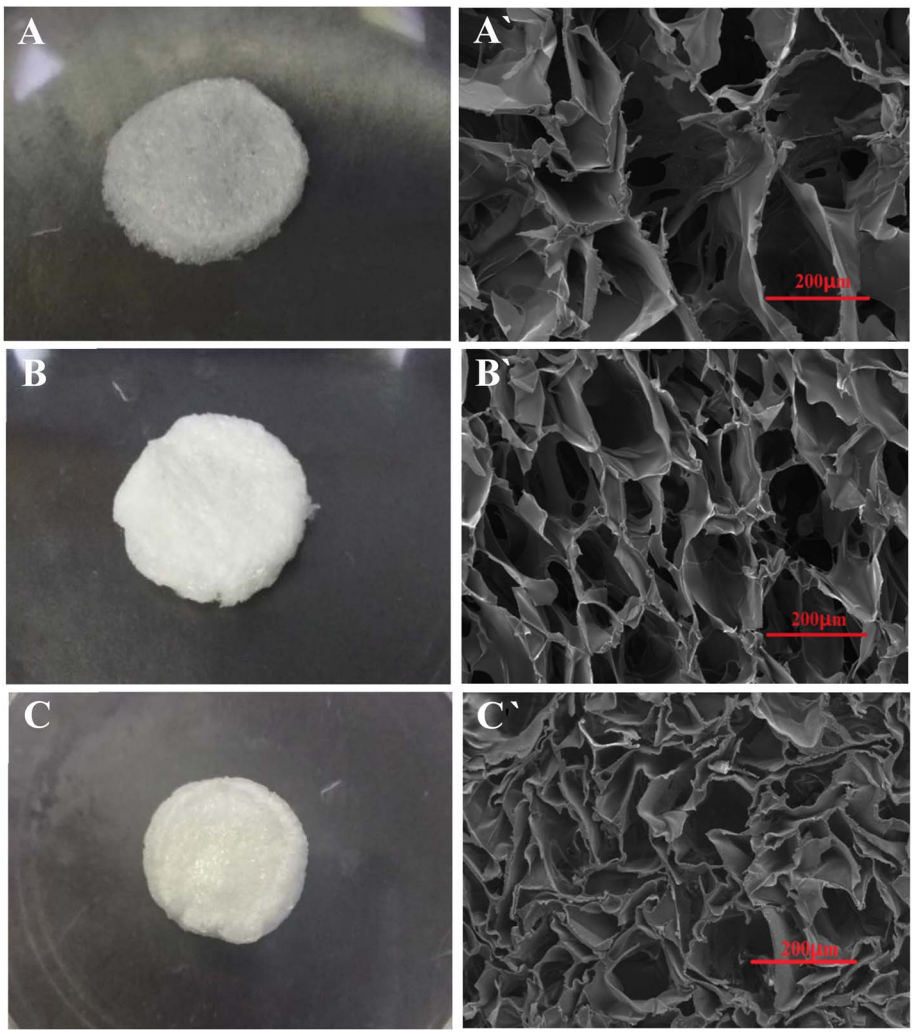

Fig. 1 Morphology and microstructure of crosslinked rCOL scaffolds (A), (B), (C) represent the morphology of crosslinked recombinant collagen scaffold materials (rCOL); (A′), (B′), (C′) represent the micro-structure of the scaffold materials (scale = 200 μm); (A) and (A′) represent crosslinked 2% rCOL scaffold; (B) and (B′) represent crosslinked 4% rCOL scaffold; (C) and (C′) represent crosslinked 8% rCOL scaffold.

Table 2 Porosity, pore size, cross-linking degree and mechanical strength of crosslinked recombinant collagen scaffolds (rCOL) (mean ± SD, $n = 6$)[a]

Sample	Porosity (%)	Pore size (μm)	Cross-linking degree (%)	Mechanical strength (N)	
				2.5 N	5 N
Crosslinked rCOL (2%)	97.8 ± 4.1%	351.2 ± 48.3	13.2 ± 3.2%	√	—
Crosslinked rCOL (4%)	95.2 ± 3.4%	185.5 ± 31.1	20.3 ± 2.8%	√	√
Crosslinked rCOL (8%)	91.1 ± 3.9%	80.6 ± 22.5	22.1 ± 3.1%	√	√

[a] "—" indicates that the material broke under the applied force."√" indicates that the material withstood this force.

scaffold C′ (crosslinked rCOL at 8% concentration) featured small, densely packed pores (Fig. 1A′–C′).

3.2 Porosity and pore size

All crosslinked rCOL scaffolds exhibited a porosity exceeding 90%, with rCOL (2%) scaffold, crosslinked at a rCOL concentration of 2%, showing the highest porosity of 97.8%. Collagen-based scaffolds with a high porosity allow efficient material exchange with the surrounding environment while providing ample space for cell expansion, making them ideal for tissue repair and regeneration.[14] Although the pore size ranged from 100 to 400 μm across all scaffolds, the average pore size showed an inverse correlation with the rCOL concentration used for crosslinking. Higher rCOL concentrations resulted in smaller pore sizes. Specifically, rCOL (4%) scaffold, crosslinked at a rCOL concentration of 4%, showed an average pore size of 185.5 ± 31.1 μm (Table 2), which was optimal for cell proliferation, aligning with the reported range of 100–300 μm for effective cell adhesion and growth.[10]

3.3 Crosslinking degree and mechanical strength

Tissue engineering materials with moderate mechanical properties exhibit excellent structural integrity and enhanced clinical operability. Ghodbane *et al.* reported that EDC/NHS crosslinking significantly enhanced the mechanical properties of animal-derived collagens and boosted their resistance to enzymatic hydrolysis.[15] Sun *et al.* found that both chemical and dehydrothermal crosslinking treatments enhanced the structural stability of fish skin collagen, with chemically crosslinked collagen demonstrating a higher crosslinking degree than its dehydrothermally crosslinked counterpart, resulting in superior tensile properties.[16] Moreover, neither crosslinking treatment altered the core structure of collagen or compromised its biological function as a wound dressing. In this study, it was found that the crosslinking degree increased with rCOL concentration, exceeding 20% for both 4% and 8% rCOL. In addition, crosslinked 4% and 8% rCOL scaffolds exhibited greater mechanical strength than crosslinked 2% rCOL scaffolds, demonstrating resistance to breaking under forces of up to 5 N (with >0.5 N considered acceptable)[17] (Table 2).

3.4 Mutagenic toxicity

Coral collagen scaffolds have demonstrated excellent biocompatibility and safety as an implantable long-term medical device.[18] In this study, the mutagenic toxicity of the crosslinked 8% rCOL scaffolds was evaluated using the Ames test. It was found that, under both activated and non-activated conditions, the number of revertant colonies in the rCOL scaffold groups did not exceed twice that of their respective negative controls, indicating negative test results for the rCOL scaffolds (Table 3). Thus, the crosslinked rCOL scaffolds exhibited no mutagenic effects on *Salmonella typhimurium*, demonstrating excellent biological safety.

3.5 Bacterial endotoxins

Bacterial endotoxin contamination of implantable medical materials can lead to serious short and long-term

Table 3 Statistical results of the number of reverse mutation colonies in each group (cfu per plate, mean ± SD, $n = 3$)[a]

Group	TA97a		TA98		TA100		TA102		TA1535	
	−S9	+S9	−S9	+S9	−S9	+S9	−S9	+S9	−S9	+S9
Experimental group 1 (0.9% sodium chloride solution extract)	223 ± 19	184 ± 3	15 ± 5	25 ± 5	210 ± 5	338 ± 47	285 ± 33	442 ± 18	8 ± 2	17 ± 5
Experimental group 2 (DMSO extract)	120 ± 15	185 ± 26	12 ± 4	34 ± 10	219 ± 18	347 ± 36	367 ± 18	502 ± 22	12 ± 3	18 ± 6
Spontaneous reverse mutant group	130 ± 3	180 ± 26	18 ± 3	22 ± 2	222 ± 13	319 ± 17	299 ± 5	450 ± 32	13 ± 3	12 ± 2
Negative control group 1 (0.9% sodium chloride)	122 ± 15*	181 ± 7*	14 ± 3*	23 ± 9*	221 ± 23*	329 ± 16*	300 ± 18*	456 ± 11*	9 ± 4*	18 ± 7*
Negative control group 2 (DMSO solution)	119 ± 14*	172 ± 26*	15 ± 5*	25 ± 7*	226 ± 15*	338 ± 13*	319 ± 16*	452 ± 30*	12 ± 7*	16 ± 1*
Positive control group	935 ± 63	446 ± 29	498 ± 63	234 ± 6	953 ± 76	631 ± 14	995 ± 179	768 ± 17	822 ± 93	179 ± 28

[a] * indicates $P < 0.05$, compared with positive control group. *Salmonella typhimurium* strains were TA97a, TA98, TA100, TA102, TA1535, respectively. −S9, without S9; +S9, with S9.

Table 4 Endotoxin test results of crosslinked recombinant collagen scaffolds (rCOL)[a]

	Crosslinked rCOL (2%)		Crosslinked rCOL (4%)		Crosslinked rCOL (8%)	
Test solution	−	−	−	−	−	−
Positive control	+	+	+	+	+	+
Test subjects positive control	+	+	+	+	+	+
Negative control	−	−	−	−	−	−

[a] "+" represents gel, "−" represents not gel.

complications. The limit of endotoxin level in implantable medical devices used in adults is commonly set at 0.5 EU per mL or 20 EU per device.[19,20] In this study, the bacterial endotoxin levels in the crosslinked rCOL scaffolds were determined using the gel-clot method. The results indicated that the endotoxin levels in the extracts of all rCOL scaffolds were below 0.5 EU per mL (<20 EU per scaffold) (Table 4), complying with the biological safety standards for implantable medical devices. Notably, the crosslinked rCOL scaffolds showed no noticeable effects on T lymphocyte proliferation and demonstrated good biological safety in delayed-type hypersensitivity reactions[9] [SI 2].

3.6 Cell adhesion and proliferation

Crosslinked collagen nanoparticles and hydrogels can significantly enhance the adhesion, proliferation, and migration of inoculated cells.[21,22] In this study, MTT staining performed 24 h after cell inoculation revealed cell growth within the 3D rCOL scaffolds, as indicated by the presence of black and purple-colored areas (Fig. 2A′). Additionally, SEM and HE staining confirmed L929 cell expansion within the pores of the rCOL scaffolds (Fig. 2B and C). A large number of proliferating cells were observed adhering to the scaffold surface, and there were filamentous extracellular matrix deposits around the cells. Notably, cell proliferation extended deep into the 3D architecture of the scaffolds, demonstrating excellent cytocompatibility and suitability as tissue regeneration and wound repair materials.

A 7-day time course study showed time-dependent cell expansion within all scaffolds (Fig. 3). Among them, the cell control group overgrew the pore plate on day 3, began to form contact inhibition and entered the plateau stage, and the cell number gradually began to decline on day 5. The number of cells in the rCOL scaffold with different concentrations and pore sizes increased steadily with the extension of time, and the cell proliferation rate in the crosslinked rCOL scaffold group with 4% concentration was the highest, which exceeded the number of cells in other groups on the 5th day, and was significantly higher than that in the control group on the 7th day (Fig. 3B, $P < 0.05$). This suggests that the scaffolds in this study can provide a good physical environment for cell growth, and the pore size may be a key factor influencing cell proliferation efficiency.[23] The proportion of hydrophilic amino acids in the rCOL sequence might be another factor affecting cell proliferation efficiency, as these residues can promote favorable cell behavior through interactions with water.[24,25] Additionally, the rCOL protein incorporated an increased number of GPP-containing sequences that are important for fibroblast adhesion and proliferation. Finally, the good mechanical properties of the crosslinked rCOL scaffolds—achieved by optimizing the spatial distribution and molar ratio of lysine and glutamic acid to facilitate more effective cross-linking [SI 1]—may have supported cell growth by providing a stable structural framework. It was noted that the proliferation rate of the control cell group was higher than that of the crosslinked rCOL scaffold groups on day 3. This was likely due to the relatively low cell distribution density of the cells in 3D environment at the beginning of the experiment.[26] The crosslinked scaffold from 8% rCOL, which had a pore size of 80.6 ± 22.5 μm, showed a lower cell proliferation rate than the 4% rCOL scaffold, which had a pore size of 185.5 ± 31.1 μm. This aligned with previous findings that a smaller pore size may limit cell attachment and differentiation within the scaffold.[27,28]

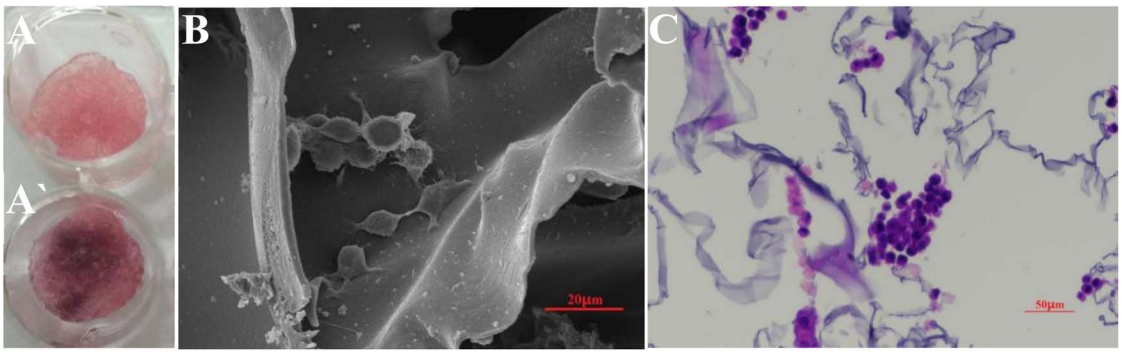

Fig. 2 Growth and adhesion status of cells on crosslinked rCOL scaffolds (4% rCOL) (A) control group (only materials); (A′) MTT staining results of cells cultured in the material for 24 h. (B) Observation of cell adhesion by scanning electron microscopy showing the status of cellular attachments (scale = 20 μm). (C) Routine histological observations of cell adhesion and proliferation in matrices (scale = 50 μm). It showed that the cells were clustered in the scaffold material space and the collagen fibers were evenly dispersed.

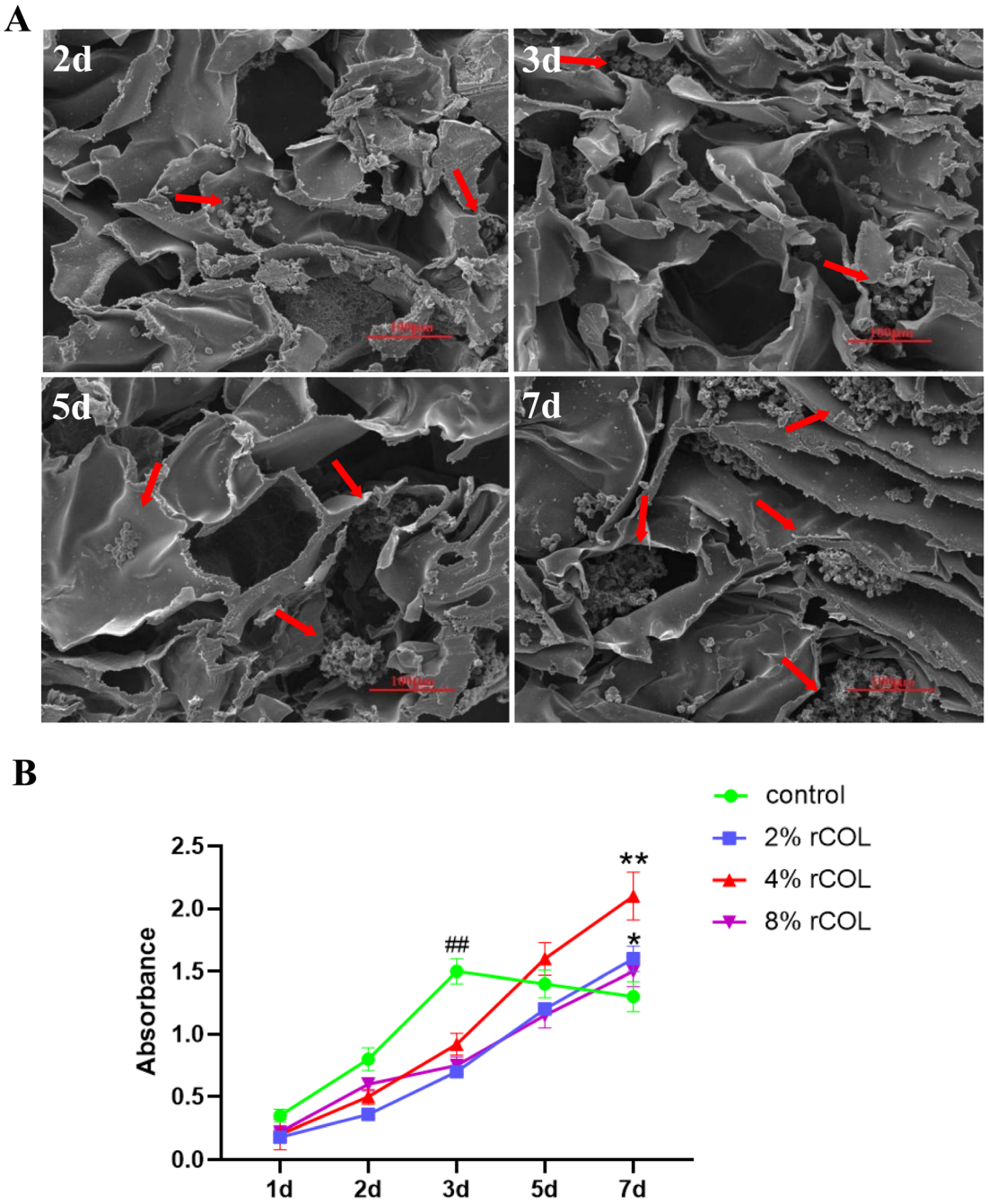

Fig. 3 Cell distribution and cell proliferation of crosslinked rCOL scaffolds (A), cell distribution in crosslinked rCOL scaffolds (4% rCOL) under scanning electron microscope for different times (red arrows indicate cell proliferation and aggregation; scale = 100 μm); (B), cell proliferation curves of crosslinked rCOL scaffolds at different concentrations (**P < 0.01, compared with other groups; *P < 0.05, compared with control group; $^{\#\#}P$ < 0.01, compared with rCOL scaffold groups).

3.7 Skin wound repair in rats

Collagen is abundantly distributed in both soft and hard connective tissues, and its effectiveness as a scaffold for wound healing has been well established. Collagen-based implants have been used as carriers for delivering cultured keratinocytes and therapeutic agents for skin replacement and burn treatment.[29,30] The hydrophilic nature of collagen plays a vital role in facilitating fibroblast infiltration during skin injury repair.[31,32] Sun and colleagues developed a collagen-based double-layer wound dressing that effectively accelerated re-epithelialization and achieved complete wound closure within 4 weeks in a full-thickness skin wound rat model.[33] Ben and colleagues reported that a recombinant human collagen hydrogel exhibited wound healing efficacy comparable to that of a humanized skin xenograft in patients with partial-thickness burns.[34] Cheng and colleagues used chemical crosslinking to enhance the water

absorption capacity of collagen sponges, improving their suitability for wound dressing applications.[35] In this study, implantation of crosslinked rCOL scaffolds or animal-derived collagen accelerated skin wound closure in rats, with crosslinked rCOL scaffolds showing significantly greater efficacy compared to animal-derived collagen 14 days post-treatment (Fig. 4A–D). Notably, the rCOL used in this study contained a higher proportion of hydrophilic amino acids than animal collagens, and the EDC/NHS-crosslinked rCOL scaffolds showed enhanced water absorption capacity than animal collagen sponges [SI 1]. In our previous research conducted in a rat model, these chimeric rCOL scaffold materials showed significant degradation by 4 weeks and were nearly completely degraded by 8 weeks after implantation, demonstrating their good biodegradability. Also, we detected no significant increases in serum IgG and IgM levels after the implantation, indicating a low immunogenicity of these materials[9] [SI 2].

When a collagen sponge is used as a dermal matrix for skin repair, fibroblasts migrate and new capillaries form in the basal layer of the collagen sponge, promoting the formation of new collagen fibers and skin structures within 2–3 weeks.[36] In this study, HE staining revealed a regenerated epidermis with newly formed dermal collagen fibers 14 days after implantation treatment. In the crosslinked rCOL scaffold treatment group, a small number of hair follicles, sebaceous glands, and other accessory structures were observed, with the skin structure gradually regenerating from the wound edges to the center (Fig. 4E). In contrast, the wound beds in both the rCOL scaffold group and control groups were primarily filled with granulation tissue (Fig. 4F and G). These results demonstrated the superior efficacy of the crosslinked rCOL scaffold in promoting tissue regeneration. This excellent wound healing effect may be attributed to its unique protein sequence design (enriched in hydrophilic amino acids and GPP-containing sequences). In

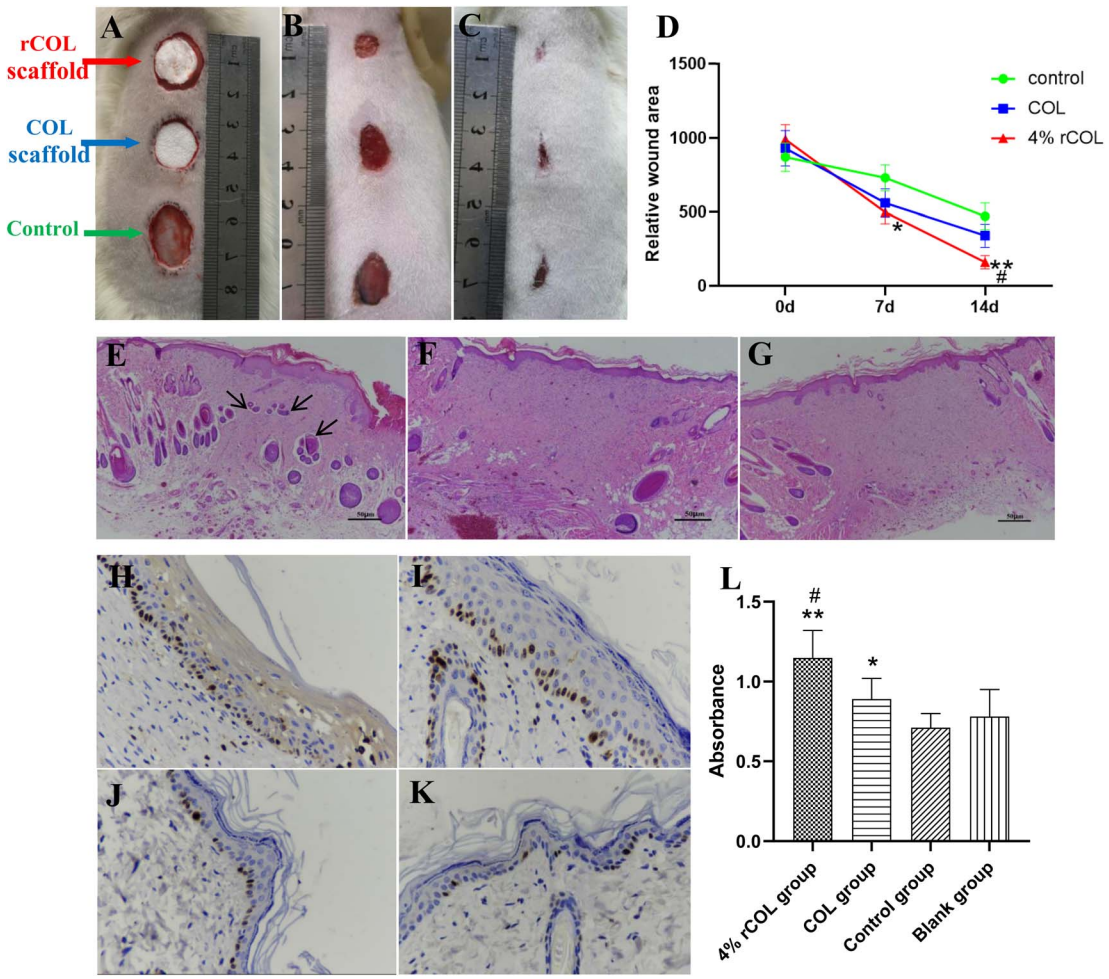

Fig. 4 Wound repair results of crosslinked rCOL scaffolds in rats (4% rCOL). At different time points (A) immediately, (B) 7 days, (C) 14 days, the wound repair status of full-layer skin defect on the back of rats; (D) skin defect area histogram at different time points; (E), (F) and (G) HE staining results of the wound at 14 days in rCOL scaffold group, COL scaffold group and untreated group, respectively (scale = 50 μm). The black arrows indicate the newly formed hair follicles and sebaceous glands. (H–K) Immunohistochemical staining results of Ki-67 in 4% rCOL scaffold group, a COL group, untreated (control) group and normal group, respectively (100×). (L) Histograms of Ki-67 immunohistochemical staining for different groups (**P < 0.01, *P < 0.05, compared with control group; #P < 0.05, compared with COL group). COL, commercially available animal-derived collagen scaffold; control group, the untreated group; blank group, the healthy unwounded skin group.

a full-thickness skin wound rat model, recombinant collagen hydrogel applied as wound dressing not only accelerated wound healing and angiogenesis, but also reduced collagen hyperplasia and scar formation.[37] Previous studies have shown that the freeze-drying protocol used in collagen sponge preparation can significantly influence their effectiveness in promoting cell growth and tissue regeneration.[38–40] In this study, a patented freeze-drying protocol was employed to effectively control the rate of ice crystal formation and sublimation during the preparation of crosslinked rCOL scaffolds. The scaffold material produced through this freeze-drying process exhibited suitable porosity and pore size to support cell attachment and proliferation (see Section 3.2 and Section 3.6). This likely helped the scaffold to enhance the wound healing capacity. Clinical studies have also demonstrated that collagen sponges with duck foot-like pore structures exhibit excellent wound repair efficacy and resistance to scar formation, making them an ideal dermal substitute for treating full-thickness skin wounds.[41]

In this study, the expression levels of Ki-67, a marker for proliferating cells, in the regenerated skin tissue of both the crosslinked rCOL scaffold and animal-derived collagen group were higher than that in the blank group, consistent with their enhanced capacity to promote wound healing. In addition, Ki-67 expression in rCOL group was significantly higher than that in animal-derived collagen group (Fig. 4L, $P < 0.05$). It was suggested that the rCOL scaffold has better effect on promoting cell proliferation and tissue repair, further supporting the possibility for use in guiding tissue regeneration and repair.

4. Conclusions

A novel chimeric rCOL composed of human type I and III sequences was used to fabricate EDC/NHS cross-linked rCOL scaffolds using a patented technology. These scaffolds demonstrated high porosity, good mechanical strength, and no genotoxicity, with endotoxin levels below the regulatory limit for implantable medical products. *In vitro*, 4% rCOL scaffolds exhibited remarkable cell adhesion and proliferation capabilities. Furthermore, in a full-thickness skin wound rat model, 4% rCOL scaffolds showed superior efficacy in promoting wound healing compared to animal-derived collagen (commercially available collagen repair products). Therefore, the crosslinked rCOL scaffolds can be used as a new type of wound repair product for further development and clinical application.

5. Limitations

This study did not evaluate the effects of the chimeric rCOL scaffolds on key fibrogenic and wound healing markers, such as Col α(I), α-SMA, TGF-β1, and vimentin. Furthermore, a comparative analysis between the chimeric rCOL scaffolds and animal-derived collagen scaffolds—regarding porosity, mechanical properties, cross-linking efficiency, and cell adhesion—was not conducted. These aspects will be addressed in future studies.

Author contributions

Yue He: conceptualization, methodology, writing – original draft preparation; Xin Wang: methodology; Yuhong Niu: supervision, validation; Jiuna Wang: writing – original draft preparation, validation; Xuyuan Yang: writing – reviewing and editing; Yongai Zhang: project administration, resources.

Conflicts of interest

The authors declare that they have no competing interests.

Data availability

The data that support the findings of this study are available from the corresponding author upon reasonable request.

Supplementary material 1. Patent AU202010052422.9. Recombinant collagen and recombinant collagen sponge material. Supplementary material 2. Evaluation of immunogenicity and *in vivo* degradation of rCOL scaffold material. Supplementary information is available. See DOI: **https://doi.org/10.1039/d5ra04354a**.

Acknowledgements

This research was funded by "Support Plan for Sanqin Scholars Innovation Team" ([2020] 45), Shaanxi province. We thank Medjaden Inc. for scientific editing of this manuscript.

References

1 M. Brown, J. Li, C. Moraes, M. Tabrizian and N. Y. K. Li-Jessen, Decellularized extracellular matrix: New promising and challenging biomaterials for regenerative medicine, *Biomaterials*, 2022, **289**, 121786.
2 C. Dong and Y. Lv, Application of Collagen Scaffold in Tissue Engineering: Recent Advances and New Perspectives, *Polymers*, 2016, **8**, 42.
3 Y. Wang, Z. Wang and Y. Dong, Collagen-Based Biomaterials for Tissue Engineering, *ACS Biomater. Sci. Eng.*, 2023, **9**, 1132–1150.
4 A. Hernández-Rangel and E. S. Martin-Martinez, Collagen based electrospun materials for skin wounds treatment, *J. Biomed. Mater. Res., Part A*, 2021, **109**, 1751–1764.
5 D. A. Yeung and N. H. Kelly, The Role of Collagen-Based Biomaterials in Chronic Wound Healing and Sports Medicine Applications, *Bioengineering*, 2021, **8**, 8.
6 S. A. Müller, L. Dürselen, P. Heisterbach, C. Evans and M. Majewski, Effect of a Simple Collagen Type I Sponge for Achilles Tendon Repair in a Rat Model, *Am. J. Sports Med.*, 2016, **44**, 1998–2004.
7 J. C. Munyemana, H. He, C. Fu, Y. Fan, X. Sun and J. Xiao, Recombinant Collagen-Templated Biomineralized Synthesis of Biocompatible pH-Responsive Porous Calcium Carbonate Nanospheres, *ACS Omega*, 2023, **8**, 30879–30887.

8 Y. Wang, F. Z. Cui, K. Hu, *et al.*, Bone regeneration by using scaffold based on mineralized recombinant collagen, *J. Biomed. Mater. Res., Part B*, 2008, **86**, 29–35.
9 Y. He, J. Wang, Y. Si, X. Wang, H. Deng, Z. Sheng, Y. Li, J. Liu and J. Zhao, A novel gene recombinant collagen hemostatic sponge with excellent biocompatibility and hemostatic effect, *Int. J. Biol. Macromol.*, 2021, **178**, 296–305.
10 Y. He, Z. Hou, J. Wang, Z. Wang, X. Li, J. Liu, X. Yang, Q. Liang and J. Zhao, Assessment of biological properties of recombinant collagen-hyaluronic acid composite scaffolds, *Int. J. Biol. Macromol.*, 2020, **149**, 1275–1284.
11 I. Prasertsung, R. Mongkolnavin, S. Kanokpanont and S. Damrongsakkul, The effects of pulsed inductively coupled plasma (PICP) on physical properties and biocompatibility of crosslinked gelatin films, *Int. J. Biol. Macromol.*, 2010, **46**, 72–78.
12 ISO 10993-3, *Biological Evaluation of Medical Devices Part 3: Tests for Genotoxicity, Carcinogenicity and Reproductive Toxicity*, 2014.
13 Chinese Pharmacopoeia, *Part 1143 Bacterial Endotoxin Test – Gel Method*, 2020.
14 S. S. Mathew-Steiner, S. Roy and C. K. Sen, Collagen in Wound Healing, *Bioengineering*, 2021, **8**, 63.
15 S. A. Ghodbane and M. G. Dunn, Physical and mechanical properties of cross-linked type I collagen scaffolds derived from bovine, porcine, and ovine tendons, *J. Biomed. Mater. Res., Part A*, 2016, **104**, 2685–2692.
16 L. Sun, B. Li, D. Yao, W. Song and H. Hou, Effects of cross-linking on mechanical, biological properties and biodegradation behavior of Nile tilapia skin collagen sponge as a biomedical material, *J. Mech. Behav. Biomed. Mater.*, 2018, **80**, 51–58.
17 YY/T 1511-2017, Medical industry standard for medical devices – Collagen Sponge.
18 D. Benayahu, L. Pomeraniec, S. Shemesh, S. Heller, Y. Rosenthal, L. Rath-Wolfson and Y. Benayahu, Biocompatibility of a Marine Collagen-Based Scaffold In Vitro and In Vivo, *Mar. Drugs*, 2020, **18**, 420.
19 GB/T 14233.2, *Test Methods for Medical Infusion, Blood Transfusion and Injection Apparatus-Part 2: Biological Experimental Methods*, 2022.
20 U.S. Pharmacopeia 40, *161: Medical Devices-Biological Tests: Bacterial Endotoxin and Pyrogen Tests*, 2017.
21 F. Ziaei Amiri, Z. Pashandi, N. Lotfibakhshaiesh, M. J. Mirzaei-Parsa, H. Ghanbari and R. Faridi-Majidi, Cell attachment effects of collagen nanoparticles on crosslinked electrospun nanofibers, *Int. J. Artif. Organs*, 2021, **44**, 199–207.
22 H. He, N. Wei, Y. Xie, L. Wang, L. Yao and J. Xiao, Self-Assembling Triple-Helix Recombinant Collagen Hydrogel Enriched with Tyrosine, *ACS Biomater. Sci. Eng.*, 2024, **10**, 3268–3279.
23 L. Huang, L. Zhu, X. Shi, B. Xia, Z. Liu, S. Zhu, Y. Yang, T. Ma, P. Cheng, K. Luo, J. Huang and Z. Luo, A compound scaffold with uniform longitudinally oriented guidance cues and a porous sheath promotes peripheral nerve regeneration in vivo, *Acta Biomater.*, 2018, **68**, 223–236.
24 F. Yang, S. Jin and Y. Tang, Marine Collagen Peptides Promote Cell Proliferation of NIH-3T3 Fibroblasts via NF-κB Signaling Pathway, *Molecules*, 2019, **24**, 4201.
25 R. A. Que, J. Arulmoli, N. A. Da Silva, L. A. Flanagan and S. W. Wang, Recombinant collagen scaffolds as substrates for human neural stem/progenitor cells, *J. Biomed. Mater. Res., Part A*, 2018, **106**, 1363–1372.
26 B. J. Kim, S. Zhao, R. P. Bunaciu, A. Yen and M. Wu, A 3D in situ cell counter reveals that breast tumor cell (MDA-MB-231) proliferation rate is reduced by the collagen matrix density, *Biotechnol. Prog.*, 2015, **31**, 990–996.
27 F. J. O'Brien, B. A. Harley, I. V. Yannas and L. J. Gibson, The effect of pore size on cell adhesion in collagen-GAG scaffolds, *Biomaterials*, 2005, **26**, 433–441.
28 C. M. Murphy and F. J. O'Brien, Understanding the effect of mean pore size on cell activity in collagen-glycosaminoglycan scaffolds, *Cell Adhes. Migr.*, 2010, **4**, 377–381.
29 S. Chattopadhyay and R. T. Raines, Review collagen-based biomaterials for wound healing, *Biopolymers*, 2014, **101**, 821–833.
30 W. Peng, D. Li, K. Dai, Y. Wang, P. Song, H. Li, P. Tang, Z. Zhang, Z. Li, Y. Zhou and C. Zhou, Recent progress of collagen, chitosan, alginate and other hydrogels in skin repair and wound dressing applications, *Int. J. Biol. Macromol.*, 2022, **208**, 400–408.
31 D. Brett, A Review of Collagen and Collagen-based Wound Dressings, *Wounds*, 2008, **20**, 347–356.
32 M. F. P. Graça, S. P. Miguel, C. S. D. Cabral and I. J. Correia, Hyaluronic acid-Based wound dressings: A review, *Carbohydr. Polym.*, 2020, **241**, 116364.
33 L. Sun, L. Li, Y. Wang, M. Li, S. Xu and C. Zhang, A collagen-based bi-layered composite dressing for accelerated wound healing, *J. Tissue Viability*, 2022, **31**, 180–189.
34 C. Ben, X. Liu, T. Shen, Y. Song, H. Li, B. Pan, W. Hou, T. Liu, P. Luo, B. Ma, Y. Sun, S. Xiao, Z. Xia, D. Cheng and S. Zhu, A recombinant human collagen hydrogel for the treatment of partial-thickness burns: A prospective, self-controlled clinical study, *Burns*, 2021, **47**, 634–642.
35 X. Cheng, Z. Shao, C. Li, L. Yu, M. A. Raja and C. Liu, Isolation, Characterization and Evaluation of Collagen from Jellyfish Rhopilema esculentum Kishinouye for Use in Hemostatic Applications, *PLoS One*, 2017, **12**, e0169731.
36 C. Jinno, N. Morimoto, R. Ito, M. Sakamoto, S. Ogino, T. Taira and S. Suzuki, A Comparison of Conventional Collagen Sponge and Collagen-Gelatin Sponge in Wound Healing, *BioMed Res. Int.*, 2016, **2016**, 4567146.

37 T. Liu, C. Qiu, H. Lu, H. Li, S. Zhu and L. Ma, A novel recombinant human collagen hydrogel as minced split-thickness skin graft overlay to promote full-thickness skin defect reconstruction, *Burns*, 2023, **49**, 169–181.

38 S. R. Caliari and B. A. Harley, The effect of anisotropic collagen-GAG scaffolds and growth factor supplementation on tendon cell recruitment, alignment, and metabolic activity, *Biomaterials*, 2011, **32**, 5330–5340.

39 H. Lu, Y. G. Ko, N. Kawazoe and G. Chen, Cartilage tissue engineering using funnel-like collagen sponges prepared with embossing ice particulate templates, *Biomaterials*, 2010, **31**, 5825–5835.

40 M. Onuma-Ukegawa, K. Bhatt, T. Hirai, H. Kaburagi, S. Sotome, Y. Wakabayashi, S. Ichinose, K. Shinomiya, A. Okawa and M. Enomoto, Bone Marrow Stromal Cells Combined With a Honeycomb Collagen Sponge Facilitate Neurite Elongation In Vitro and Neural Restoration in the Hemisected Rat Spinal Cord, *Cell Transplant.*, 2015, **24**, 1283–1297.

41 M. T. Sultan, J. Y. Jeong, Y. B. Seo, O. J. Lee, H. W. Ju, H. J. Park, Y. J. Lee, J. S. Lee, S. H. Kim and C. H. Park, Fabrication and characterization of the porous duck's feet collagen sponge for wound healing applications, *J. Biomater. Sci. Polym. Ed.*, 2018, **29**, 960–971.